Estudios Geológicos 81(2)
julio-diciembre 2025, 1143
ISSN-L: 0367-0449
https://doi.org/10.3989/egeol.45761.1143

Role of colloids in the dispersion of arsenic in mine soils from Madrid

Papel de los coloides en la dispersión de arsénico en suelos de mina de Madrid

Miguel Ángel Gómez-González[1], Fernando Garrido[2]*, Francisco Laborda[3], Mario Villalobos[4], Eduardo Bolea[3], Paula Gómez-Arce[2], Javier Aguilar-Carrillo[5]

[1] Diamond Light Source Synchrotron. Beamline I14. Didcot, Oxfordshire, OX11 0DE, United Kingdom. https://orcid.org/0000-0003-2725-4820
[2] Museo Nacional de Ciencias Naturales, CSIC. José Gutiérrez Abascal 2. 28006-Madrid. https://orcid.org/0000-0002-7491-3780, https://orcid.org/0000-0003-3728-947X
[3] Grupo de Espectroscopía Analítica y Sensores (GEAS). Instituto U. de Investigación en Ciencias Ambientales de Aragón (IUCA). Universidad de Zaragoza. Pedro Cerbuna, 12. 50009-Zaragoza. https://orcid.org/0000-0002-4169-0357, https://orcid.org/0000-0001-5382-0561
[4] Laboratorio de Geoquímica Ambiental Molecular, LANGEM, Instituto de Geología. UNAM, Coyoacán, 04510, Ciudad de México, México. https://orcid.org/0000-0003-2820-848X
[5] Universidad Autónoma de San Luis Potosí. Instituto de Metalurgia. Av. Sierra Leona 550 Lomas 2a. Sección CP. 78210 San Luis Potosí, México. https://orcid.org/0000-0002-5341-3381
*Correspondencia: fernando.garrido@mncn.csic.es

ABSTRACT

In recent years, elevated concentrations of arsenic (As) have been detected in the Tertiary detrital aquifer of Madrid. A significant number of areas where waste from old mining operations, rich in metals and metalloids, accumulate may partially explain contamination events by toxic elements. In these environments, colloidal particles can act as nanovectors for the dispersion of As, enhancing its migration and contamination of surrounding soils. This work studies the mobilization of As-rich colloids from a waste zone of an old mining operation in the Community of Madrid. These wastes, mainly composed of arsenopyrite [FeAsS] ([As] = 0.2 g kg^{-1}), are deposited near a natural stream and exposed to environmental conditions. In order to follow the mobility of As-rich colloids, the combined techniques of asymmetric flow field flow fractionation and inductively coupled plasma mass spectrometry (AF4-ICP-MS) are used to obtain the size distribution of the colloidal fraction and associated As, while X-ray absorption spectroscopy (XAS) techniques are utilized for the study of the chemical speciation of As in the solid phase. In addition, geochemical modeling allows prediction of the thermodynamically favored phases in each of the studied areas. The mobilization of colloidal As from mining waste to water and soil located up to 1 km from the source of contamination is described. The essential role of colloidal Fe oxyhydroxides as As mobilizing nanovectors is also highlighted.

Keywords: Arsenic; Colloids; XAS; AF4-ICP-MS; Mine wastes.

Recibido el 14 de abril de 2025; Aceptado el 3 de junio de 2025; Publicado online el 11 de diciembre de 2025.

Cómo citar: Gómez-González, M. A., Garrido, F., Laborda, F., Villalobos, M., Bolea, E, Gómez-Arce, P. & Aguilar-Carrillo, J. (2025). Role of colloids in the dispersion of arsenic in mine soils from Madrid *Estudios Geológicos*, 81(2), 1143. https://doi.org/10.3989/egeol.45761.1143

RESUMEN

Durante los últimos años se han detectado concentraciones elevadas de arsénico (As) en el acuífero detrítico terciario de Madrid. Un número importante de zonas de acumulación de residuos de antiguas explotaciones mineras ricas en metales y metaloides pueden explicar parcialmente eventos de contaminación por elementos tóxicos. En estos entornos, las partículas coloidales pueden funcionar como nanovectores de dispersión de As potenciando su migración y contaminación de suelos colindantes. En este trabajo se estudia el proceso de movilización de coloides ricos en As a partir de una zona de residuos de una antigua explotación minera en la Comunidad de Madrid. Estos residuos, compuestos principalmente por arsenopirita [FeAsS] ([As] = 0.2 g kg^{-1}), están depositados en las cercanías de un arroyo natural y expuestos a las condiciones ambientales. Para investigar la movilización de coloides ricos en As, se emplea la técnica combinada de fraccionamiento en flujo por campo de flujo asimétrico y espectrometría de masas con plasma de acoplamiento inductivo (AF4-ICP-MS) con la que se obtiene la distribución por tamaños de la fracción coloidal y de As asociado, técnicas de espectroscopia de absorción de rayos X (XAS) para el estudio de la especiación química del As en fase sólida y programas de modelización geoquímica que permiten predecir las fases termodinámicamente favorecidas en cada una de las zonas estudiadas. Se describe la movilización de As coloidal desde el residuo minero hasta aguas y suelos situados a una distancia de 1 km del foco de contaminación. Asimismo, se pone de manifiesto el papel primordial de los oxohidróxidos de Fe coloidales como nanovectores de movilización de As.

Palabras clave: Arsénico; Coloides; XAS; AF4-ICP-MS; Residuos mineros.

Introduction

One of the main causes of trace element mobilization is the disposal and accumulation of untreated waste from mining activities on the soil. This waste often contains high concentrations of metal and arsenic sulfides that, when exposed to atmospheric conditions and erosion and upon oxidation, act as emission sources of As and other toxic species in the soil-water system (Canovas et al., 2021). These situations generate total concentrations of potentially toxic elements above natural levels in the soil (Canovas et al., 2021), which may leach dissolved fractions that easily contaminate water reserves. To prevent the spread of contamination, it is necessary to understand the natural mechanisms of contaminant release and mobility in these sites, as well as the retention processes that can reduce their toxicity, *i.e.*, the transformations and reactions that these elements undergo in the soil matrix, both with the solid and aqueous phases.

Colloidal particles are found in most natural systems, including surface waters, soil macropores, and underground aqueous systems (Kretzschmar et al., 1999). Intense rainfall generally causes rapid infiltration of waters with low ionic strength through soil macropores, leading to geochemical conditions that favor colloidal release and transport. The fundamental mechanisms of toxic element mobilization mediated by colloids and their participation in the overall soil contamination process are not sufficiently identified, which limits the development of efficient models to help remediate or prevent this soil contamination.

While As toxicity can be reduced by natural mechanisms such as association with Fe oxyhydroxides, hydroxysulfates, or precipitation as scorodite – $FeAsO_4 \cdot 2H_2O$ (Courtin-Nomade et al., 2016) or metal arsenates (Villalobos et al., 2010), various natural conditions can lead to the release of colloidal particles of these minerals, acting as inorganic vectors of As that can be transported in runoff water (Gomez-Gonzalez et al., 2016) and release the As when geochemical conditions promote it. None of these natural As uptake forms can be considered effective in reducing soil-water system contamination by As in the vicinity of mine waste when exposed to natural conditions. Although the dual transport of colloids and associated toxic elements through various geochemical mechanisms is an important mechanism of contaminant diffusion (Kretzschmar et al., 1999, Hu et al., 2023), the study of As chemical speciation in mobile colloidal particles and the distribution of As between colloids and the dissolved phase has received little attention (Serrano et al., 2015).

In order to study the colloidal vectors involved in As contamination and to identify their speciation, a combination of spectroscopic and separation analytical techniques is proposed. Asymmetrical flow field-flow fractionation (AF4) has been used for the separation and characterization of colloids (Laborda et al., 2011). Using AF4, colloids are separated according to their diffusion against a flow field applied perpendicular to the sample introduction flow (Bolea et al., 2010). When coupled with an inductively coupled plasma mass spectrometer (ICP-MS) as a detection system, the elemental composition of the colloids can be determined in addition to their size distribution (Gomez-Gonzalez et al., 2016). However, elemental

analysis does not show the chemical speciation of the metal(loid)-colloid association, which is fundamental to determining the bioavailability and toxicity of these complexes. Synchrotron radiation-based X-ray absorption spectroscopy (XAS) allows the determination of As speciation in natural samples (O'Day et al., 2004), including colloidal particles (Serrano et al., 2015). Recently, Gomez-Gonzalez et al. (2015) identified scorodite and ferric oxyhydroxide colloids as As nanovectors and their potential for metalloid transport from the emission source using a combination of XAS spectroscopy and AF4 fractionation. In this work, the speciation of As in the dispersible colloidal fraction (potentially mobile and size <1000nm) of soils located in a gorge where drainage water from mine waste exposed to atmospheric conditions flows is studied. For this purpose, an experimental protocol is applied that includes spectroscopic and fractionation techniques in addition to theoretical models of geochemical speciation, allowing the determination of the elemental composition of colloidal vectors, their mineral nature, and the speciation of As associated with these particles.

Materials and Methods

Study Area and Sampling

The Mónica Mine is located in the Sierra de Guadarrama, in the Madrid municipality of Bustarviejo (40°52'04.48" N – 3°43'48.68" W, 1475m altitude). Formed mainly of arsenopyrites (FeAsS) with matildite ($AgBiS_2$) mineralizations, it was exploited from 1427 to 1980 (Jimenez et al., 2004), producing approximately 350Kg of Ag (grade 120g/t) and 1600Kg of Cu (Martin-Crespo et al., 2004) annually. The mining waste (500m^2 and average thickness of 3m) is rich in pyrite (FeS_2), contains 22 g kg^{-1} of As, and is a source of As and other metal contamination of soils and waters (Moreno-Jiménez et al., 2009). The waste discharges its drainage water directly into a stream course along the "La Mina" gorge (Figure 1). In this environment, samples of the first 15cm of waste were taken in the area closest to the mine (WP) and about 28m away (WP-2). Similarly, soil samples were collected in seven spots along the stream bed. Samples A and B were taken near the mine, where the stream bed borders the mining waste (Figure 1). Sample C was collected in a small auxiliary channel originating from the WP-2 area and feeding the main stream. Along the stream gorge, small intermediate accumulation areas with a gentler slope are generated, which were identified as D-E-F-G. Sample G (the furthest from the contamination source) is located about 860m from the mine. Undisturbed soil columns of 15cm depth were taken at each sampling point. Additionally, eight water samples were collected from the stream in the vicinity of the mine and the WP-2 spoil heap, as well as along the stream. These samples were filtered and acidified (HNO_3, 1%), and stored at 4ºC until analysis.

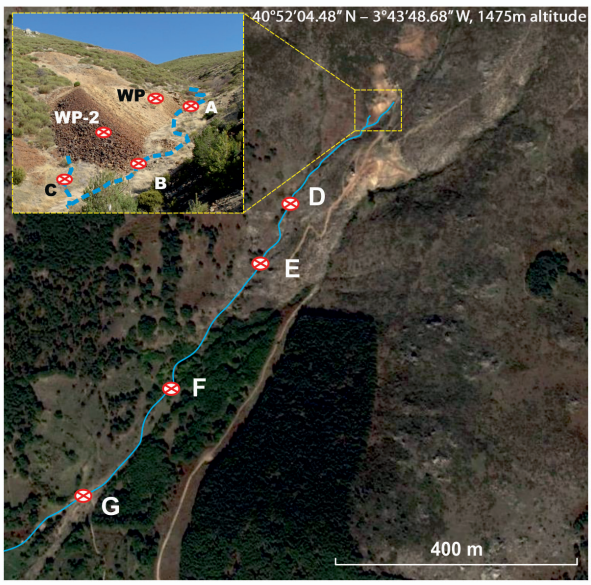

Figure 1.— Sampling points (Google Earth ®). WP: Waste pile close to Monica mine (Bustarviejo, Madrid).

Sample characterization

The solid samples were air-dried, homogenized, and sieved (<2mm). pH and electrical conductivity (EC) were determined in 1:5 w/w suspensions (deionized water) and the organic C content by wet digestion (Walkley and Black, 1934). Likewise, a semiquantitative determination of the mineralogical composition was performed on the <2mm fraction of all samples and on the clay fraction (<2μm) of four samples (WP-B-E-F) by X-ray diffraction. For this, a PW-1700/00 X-ray diffractometer (Philips) was used, Cu Kα radiation and Ni filter, applying a power and intensity of 40kV and 40mA, respectively. Quantification was performed by comparing standards from the ICDDPDF2 and DIFDATA databases.

The elemental composition of the soils was determined in duplicate by ICP-OES (iCAP 6500Duo, ThermoFisher Sci.) in filtered solutions (0.45μm, polyether-sulfone) after digestion in aqua regia (HNO_3/HCl, 1:3 ratio) in a microwave oven (Ethos S1, Milestone) (Chen and Ma, 2001). The elemental composition of the water samples was analyzed by ICP-MS (ELAN DRC-e, Perkin Elmer).

Extraction of the Dispersible Colloidal (DCF) and the Dissolved Fraction (DF)

The dispersible colloidal fraction (DCF, ≤1000nm) is defined as the maximum amount of colloids (mg kg-1 of sample) and dissolved fraction potentially released from the soil under fixed leaching conditions (Serrano et al., 2015). For its extraction, the soil sample is leached with ultrapure water (soil/water 1:10 w/w) in 24 hours of rotary stirring at room temperature, where the supernatant is the DCF (Gomez-Gonzalez et al., 2015). From this supernatant (DCF), two fractions are extracted by ultrafiltration (10nm pore size membrane, 100kDa): (1) the colloidal fraction (CF, 1000-10nm) retained on the membrane and (2) the dissolved fraction (DF, <10nm) that passes through the membrane. Several aliquots of each DCF obtained were used for determinations by AF4-ICP-MS, quantification of colloid mass (Plathe et al., 2010), and its elemental composition. For this, 10mL of the DCF are mixed in previously tared test tubes with 6 mg of NaCl. The mixture is shaken for 30 minutes and centrifuged (15', 4000 rpm). The supernatants are discarded, and the coagulated colloidal mass (dried at 60ºC, 24 hr) is determined on a precision balance (±0.001 mg).

The concentration of As and metals present in the DF was determined by ICP-MS without prior acid digestion, while the CF deposited on the ultrafiltration membranes was used to study of the molecular speciation of As and Fe by XAS.

Asymmetric Flow Field-Flow Fractionation Coupled with Inductively Coupled Plasma Mass Spectrometry (AF4-ICP-MS)

The obtained DCF was used to determine the size distribution of soil colloids. The high conductivity of samples WP and WP-2 prevented their fractionation due to the irreversible adsorption of these colloids onto the AF4 channel membrane. The DCF from samples A-B-C-D-E-F-G were measured by AF4 (AF2000, Postnova Analytics) coupled to a UV-Vis detector (Shimadzu, wavelength 200-650 nm). The AF4-UV-Vis system was coupled to an ICP-MS (Elan DRC-e, Perkin Elmer) to quantify the elemental composition of the colloids (Gomez-Gonzalez et al., 2018). The entire AF4-UV-Vis-ICP-MS system is described in Serrano et al. (2015). Reliability of the technique is evaluated through the recovery ratio (%) expressed as R(%) = Sx100/So, where S is the signal area obtained when a crossflow is applied, and So is the signal area obtained with no crossflow. Further information can be found in Gomez-Gonzalez et al. (2018).

X-ray absorption spectroscopy of As and Fe

The colloidal fractions (CF, 1000-10 nm) of selected samples (WP, B, D, F, G) were analyzed by X-ray absorption spectroscopy (XAS) on the K electronic transition of As and Fe at room temperature, using a 13-element solid-state Ge(Li) fluorescence detector (6GeV, 100mA, Si(111) monochromator; BM25A beamline, ESRF, Grenoble, France). The beam energy was calibrated to 11875eV from the

K-absorption maximum of KH_2AsO_4 (Sigma-Aldrich) for As measurements and to 7112eV from the first inflection point of a Fe(0) foil. The sample spectra were acquired from 11650eV for As and from 6950eV for Fe. The EXAFS spectrum was recorded up to 11.5Å-1 for As and up to 10.5Å-1 for Fe in the k-space of the spectrum, with constant measurements every 0.05Å-1 throughout the EXAFS. The final spectrum of each sample was obtained by averaging 10-12 replicated spectra and analyzed by linear combination fitting (LCF) with the Athena program (Ravel and Newville, 2005) along with reference spectra (16 for Fe and 12 for As) over a range of k values 2-7Å-1 for Fe and 2-10.5Å-1 for As (Gomez-Gonzalez et al., 2018).

Thermodynamically favorable mineral phases: Geochemical modeling

The stability of the chemical compounds present in the natural system was evaluated using equilibrium speciation geochemical models: Visual MINTEQ (Gustafsson, 2010), MINEQL+ (Scheder and McAvoy, 1992), and PHREEQC-v2.18 (Parkhurst and Appelo, 1999). The equilibrium formation constants of the mineral phases were reviewed and updated by Villalobos et al. (2010). These programs were used to calculate the thermodynamically favorable mineral phases, both in soil samples and in the dispersible colloidal fractions.

Results

Physico-chemical properties and elemental composition of soils and waters

The residues (WP, WP-2) exhibit higher acidity and electrical conductivity (EC) than the soil samples (A-B-C-D-E-F-G) (Table 1). The <2 mm fraction (total soil) shows a similar mineralogical composition in all cases, consisting of quartz, albite [$NaAlSi_3O_8$], and small proportions of phyllosilicates, along with jarosite [$KFe_3(SO_4)_2(OH)_6$], the latter in the case of the residues. The clay fraction of the residue differs significantly from the soil samples. In the former, montmorillonite, jarosite, illite, and kaolinite are detected as predominant minerals, while in the soil samples, illite, albite, and microcline [$KAlSi_3O_8$] dominate in varying proportions (Table 2).

Table 1. Soil samples characterizations

	WP	WP-2	A	B	C	D	E	F	G
pH	3.4	3.7	6.8	6.6	6.2	6.7	6.7	6.5	6.6
EC ***(µS cm^{-1})***	137	88.4	66.7	30.8	60.6	16.0	54.8	22.3	18.8
Total organic carbon (%)									
TOC	0.2	0.2	3.1	1.5	3.5	1.1	4.7	5.5	1.4

Table 2. Mineralogical composition of the clay fraction (<2 ***µ***m) of selected samples

Sample	M[a]	J	I	K	Q	A	Mc
	(%)						
WP	38	29	15	9	9		
B	2		62	35	1		
E	2		18	2	12	26	40
F	2		43	2	20	33	

[a]M: Montmorillonite; J: Jarosite;, I: Illite; K: Kaolinite; Q: Quartz; A: Albite; Mc: Microcline.
Maximum errors: 15% for major components,; 25% when total contribution is <20%.

The high concentration of As and other toxic elements in the mining residue stands out (Table 3). However, only the concentrations of As and Pb decrease with distance from the contamination source. Similarly, the As/Fe molar ratio decreases with distance, suggesting a greater importance of Fe oxyhydroxides in the stream bed. The water sample collected at the mine's outlet shows elevated levels of Mn, Fe, Tl, and Cu (Table 4), indicating the polluting effect of these residues on surface waters. The As concentration remains constant in the spoil heap area (Mine and WP-2) and in the stream bed near these points (A and C) but increases with distance in the rest of the samples.

Table 3. Elemental composition of the waste and soil samples

Sample	Al	Mn	Fe	Cu	Zn	As	Pb	As/ Feb
	(mg kg^{-1}) [a]							
WP	1550	364	6.9x10^4	369	365	2.2x10^4	3213	0.23
WP-2	1800	336	4.8x10^4	271	295	6934	1639	0.11
A	2950	1060	2.7x10^4	841	1297	3249	438	0.09
B	4120	957	3.4x10^4	1886	1525	3313	448	0.07
C	4900	1131	4.3x10^4	2462	1860	2944	334	0.05
D	2930	838	2.3x10^4	1383	1172	2278	354	0.07
E	3030	1312	2.3x10^4	3471	2155	2343	261	0.07
F	2440	668	2.1x10^4	360	1331	816	172	0.03
G	2140	467	1.9x10^4	281	1167	1041	182	0.04

[a] Standard deviation are (mg kg^{-1}): Al=±13.1; Mn=±1.2; Fe=±7.2; Cu=±0.7; Zn=±1.0; As=±0.3; Pb=±2.4.
[b] Molar ratio

Table 4. Streamwater chemical properties and element composition

Sample	pH	EC *(µS cm^{-1})*	Mn	Fe	As	Tl	Pb
			(µg L^{-1})				
Mine	3.9	237	204±8.8	250±31	32±1.7	0.083±0.005	14±0.3
WP-2	6.9	47.6	6.0±0.5	34±8.1	32±2.6	0.011±0.005	0.28±0.03
A	6.7	45.6	16.8±1	42±6.9	31±2.5	0.012±0.005	0.32±0.02
B	6.8	49.7	7.1±0.8	60±10	67±6.1	0.012±0.005	0.52±0.06
C	7.0	47.5	8.8±0.2	48±7.2	31±2.3	0.010±0.005	0.41±0.01
D	7.0	46.0	2.8±0.1	90±17	92±11	0.012±0.005	0.88±0.03
E	6.9	47.8	1.7±0.2	69±8.9	108±10	0.012±0.005	0.75±0.03
F	7.2	47.3	1.8±0.4	56±4.8	87±2.2	0.008±0.005	0.24±0.01

As and Fe chemical speciation through X-ray absorption spectroscopy

The analysis of K-edge EXAFS spectra (Table 5, Figure 2) for As highlights the importance of Fe(III) oxyhydroxides, such as ferrihydrite (a nanometric hydrous ferric oxide), in the adsorption of As(V), this phase is controlling the As retention in the analyzed soil samples (B-D-F-G), followed in importance by goethite (α-FeOOH). In the mining residue sample (WP), in addition to 56% retained by ferrihydrite, 26% appear as scorodite and 17% are retained by jarosite. In the case of Fe spectra, the WP sample reflects the main presence of scorodite (70%) as a byproduct of arsenopyrite oxidation from the mining residue, and chlorite [$(Mg, Fe)_3(Si,Al)_4O_{10}(OH)_2 \cdot (Mg,Fe)_3(OH)_6$] (29%), which suggests the presence of Fe(II) from this arsenopyrite in the form of mixed Fe(II)/Fe(III) oxides. However, the stream bed samples all show a mixture of illite clay (49-59%) and poorly crystalline Fe(III) hydroxysulfates (schwertmannite [$Fe_8O_8(OH)_6(SO_4)\ n\ H_2O$] 35-46%).

Table 5. Linear combination fittings of EXAFS spectra from soil samples

As_EXAFS[a]							
Sample	**As-Fh[b]** *(%)*	**Sco[c]** *(%)*	**As-Jar[d]** *(%)*	**As-Goe[e]** *(%)*	**Total[f]** *(%)*	**R[g]**	**χ^2 red.[h]**
WP	56.0	26.2	16.9		99.1	0.010	0.171
B	97.3			1.6	98.9	0.014	0.330
D	70.5			23.1	93.6	0.021	0.487
F	85.8			11.0	96.8	0.021	0.489
G	70.7			22.1	92.8	0.052	1.08
Fe_EXAFS[i]							
Sample	**Sco[c]** *(%)*	**Chlor[j]** *(%)*	**Illi[k]** *(%)*	**Schw[l]** *(%)*	**Total** *(%)*	**R[g]**	**χ^2red[h]**
WP	70.5	28.9			99.4	0.057	0.334
B			59.1	35.1	94.2	0.051	0.259
D			49.1	45.7	94.8	0.034	0.225
F			36.8	53.8	90.6	0.014	0.095

[a]LCF over k range: 2–10.5 Å for As EXAFS; [b]As(V) adsorbed on ferrihydrite; [c]Scorodite
[d]As(V) adsorbed on jarosite; [e]As(V) adsorbed on goethite; [f]Sum of phases. The sum of the reference contributions was not forced to equal 100%; [g]R=$\sum$(data-adjust)^2 / $\sum$date^2); [h]Goodness of fit; χ^2 reduced=(factor F)/(nº of points–nº of variables); [i]LCF over k range k: 2–7Å for Fe EXAFS; [j]Chlorite; [k]Illite; [l]Schwertmannite.

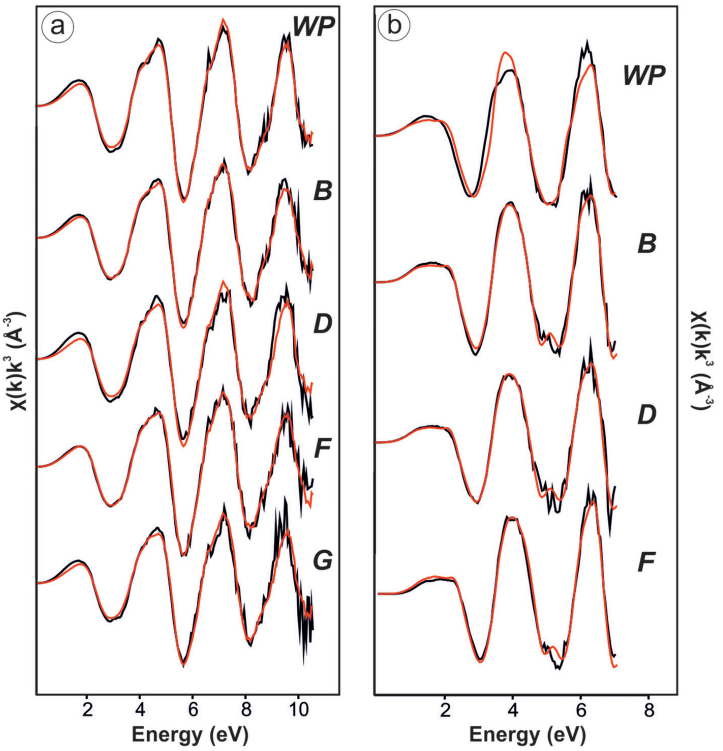

Figure 2.— EXAFS spectra of As (a) and Fe (b) in waste and soil samples. Black: experimental data; red: best linear combination fits (LCFs), according to data from Table 5.

Colloidal As and Fe speciation through X-ray absorption spectroscopy

The As EXAFS spectra of the colloidal fractions (CF) show the majority contribution of ferrihydrite as the colloidal vector of As in stream bed samples, along with minor contributions of goethite, beudantite [$PbFe_3(OH)_6SO_4AsO_4$], or jarosite. The CF of sample WP also presents a significant content

of ferrihydrite (51%), scorodite (36%), and goethite (15%) (Table 6, Figure 3). The Fe EXAFS indicate the importance of smectite and illite clays in the colloidal fraction of all samples. The presence of schwertmannite and plumbojarosite [$Pb_{0.5}Fe^{3+}_3(SO_4)_2(OH)_6$] also stands out. However, only the CF of sample B shows a contribution of ferrihydrite (66%), probably due to the greater importance of smectite and illite in samples further from the contamination source.

Table 6. Linear combination fitting of EXAFS spectra from colloid samples

As_EXAFS[a]									
Sample	**As-FH[b]** *(%)*		**Sco[c]** *(%)*	**As-Goe[d]** *(%)*	**Beud[e]** *(%)*	**As-Jar[f]** *(%)*	**Total[g]** *(%)*	**R[h]**	**χ^2 red[i]**
WP	50.8		35.9	15.1			101.8	0.017	0.438
B	97.1			6.3			103.4	0.017	0.456
D	92.3			7.8			100.1	0.022	0.552
F	90.1				13.4		103.5	0.091	2.53
G	96.3					4.2	100.5	0.041	1.02
Fe_EXAFS[j]									
Sample.	**Sme[k]** *(%)*	**Sch[l]** *(%)*	**Pb-Jar[m]** *(%)*	**Fh[n]** *(%)*	**Illi[o]** *(%)*	**Jar[f]** *(%)*	**Total[g]** *(%)*	**R[h]**	**χ^2 red[i]**
WP	36.2	34.2	33.9				104.3	0.008	0.100
B	28.0		14.1	66			108.2	0.019	0.176
D	15.6	62.9	16.0				94.5	0.006	0.058
F		58.0			26.9	20.9	105.8	0.008	0.090

[a]LCF over k range: 2–10.5Å; [b]As(V) adsorbed on ferrihydrite ; [c]Scorodite; [d]As(V) adsorbed on goethite; [e]Beudantite; [f]As(V) adsorbed on jarosite; [g]The sum of the reference contributions was not forced to equal 100%; [h]$R=\sum(\text{data-adjust})^2 / \sum\text{data}^2$); [i]Goodness of fit; χ^2 reduced=[(factor F) / (nº of points – nº of variables)]; [j]LCF over k range: 2–7Å; [k]Smectite; [l]Schwertmannite; [m]Plumbo-jarosita; [n]Ferrihydrite; [o]Illite

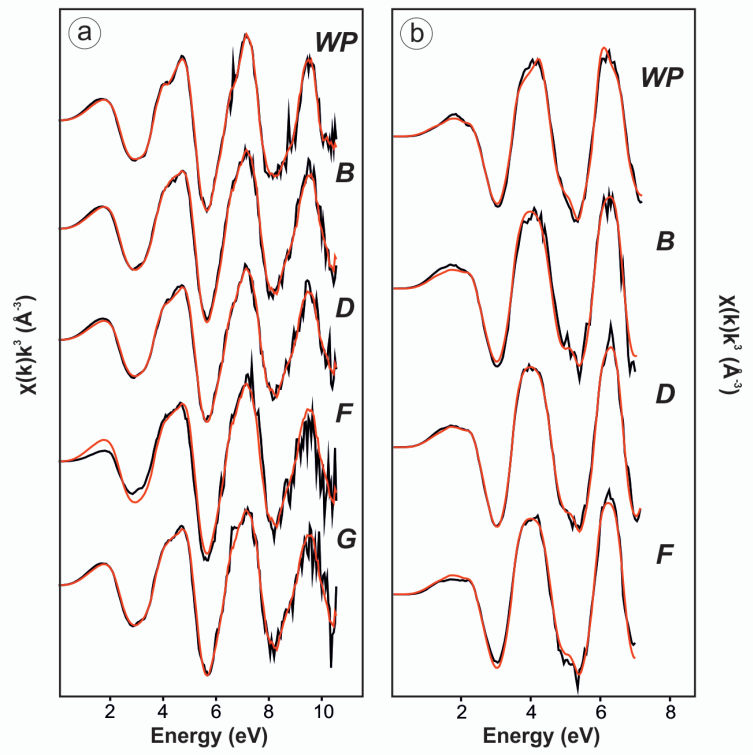

Figure 3.— EXAFS spectra of As (a) y Fe (b) in colloid samples. Black: experimental data; red: best LCFs according to data from Table 6.

Characterization of the dispersible colloidal fraction (DCF)

Table 7 shows the elemental composition of the dispersible colloidal fraction (DCF, ≤ 1000 nm), the dissolved fraction (DF, < 10 nm), and the colloidal fraction (CF, 1000-10 nm) of all samples. The CF is defined as the difference between the two previous concentrations. The low concentration of As in the DCF of the two spoil heap samples and the concentrations one order of magnitude higher in the DCF of the samples collected along the stream stand out. In general, a large proportion of the metals and As in samples A-B-C-D-E-F-G are associated with the CF, indicating the extremely low concentration of these elements in the dissolved fraction. Finally, As and Fe are the major elements in the CF of the stream samples, although significant concentrations of Cu and Pb are also found. Considering the As and Fe concentrations in the CF (Table 7), high concentrations of As and Fe per calculated colloidal mass are obtained (Table 8). The As/Fe molar ratio decreases from the DCF of samples WP and WP-2 to the DCF of the last determined samples.

Table 7. Element concentration of Dispersible colloid Fraction, Dissolved Fraction and Colloid Fraction.

Sample		As	Fe	Al	Cu	Pb
		(mg L^{-1})[a]				
WP	DCF	0.23±0.05	1.13±0.22	0.73±0.06	0.22±0.01	0.04±0.01
	DF	0.03±0.01	0.74±0.29	0.64±0.08	0.23±0.02	0.01±0.01
	CF[b]	0.20	0.39	0.09	-[c]	0.03
WP-2	DCF	0.08±0.02	0.48±0.22	0.65±0.15	0.16±0.03	0.02±0.01
	DF	0.01±0.01	0.13±0.16	0.26±0.07	0.18±0.02	0.01±0.01
	CF[b]	0.07	0.35	0.39	-[c]	0.01
A	DCF	8.67±0.14	81±0.4	104±0.1	2.86±0.09	1.65±0.34
	DF	0.12±0.04	0.03±0.03	0.06±0.03	0.06±0.03	0.01±0.01
	CF[b]	8.55	~81	~104	2.80	1.64
B	DCF	9.58±0.16	81±0.5	84±0.2	3.85±0.12	1.59±0.38
	DF	0.21±0.03	0.03±0.03	0.05±0.04	0.21±0.04	0.01±0.01
	CF[b]	9.37	~81	~84	3.64	1.58
C	DCF	2.70±0.08	31±0.7	33±0.2	1.93±0.20	0.43±0.13
	DF	0.01±0.01	0.03±0.03	0.06±0.04	0.04±0.01	0.01±0.01
	CF[b]	2.69	~31	~33	1.89	0.42
D	DCF	7.54±0.19	55±0.6	68±0.2	4.80±0.17	1.44±0.35
	DF	0.20±0.06	0.03±0.03	0.08±0.07	0.23±0.05	0.01±0.01
	CF[b]	7.34	~55	~68	4.57	1.43
E	DCF	6.76±0.12	62±0.6	79±0.4	7.24±0.19	1.20±0.20
	DF	0.16±0.07	0.03±0.03	0.05±0.03	0.32±0.04	0.01±0.01
	CF[b]	6.60	~62	~79	6.92	1.19
F	DCF	2.31±0.18	47±0.5	76±0.3	0.87±0.08	0.60±0.37
	DF	0.22±0.07	0.03±0.03	0.05±0.02	0.06±0.01	0.01±0.01
	CF[b]	2.09	~47	~76	0.81	0.59
G	DCF	1.29±0.21	24±0.3	37±0.1	0.46±0.16	0.32±0.21
	DF	0.23±0.07	0.03±0.03	0.06±0.05	0.04±0.01	0.01±0.01
	CF[b]	1.06	~24	~37	0.42	0.31

[a] Pseudototal concentration ± Standard Deviation (n=3)
[b] CF concentration(1000-10nm) = DCF (≤ 1000nm)-DF (< 10nm)
[c] Not significant concentration

Tabla 8. Colloid concentrations of the DCF and As and Fe in the colloidal (CF), normalized per mass

Sample	Colloids	As	Fe	As/Fe[c]
	(g kg^{-1})[a]	*(g kg-colloid^{-1})*[b]		
WP	1.4±0.3	1.43	2.80	0.15
WP-2	2.1±0.2	0.34	1.70	0.12
A	8.8±0.6	9.73	9.21	0.08
B	9.2±0.4	10.18	87.99	0.09
C	6.4±0.5	4.21	48.54	0.06
D	7.7±0.6	9.48	71.02	0.10
E	8.9±0.1	7.42	69.1	0.08
F	8.0±0.5	2.62	58.83	0.04
G	7.9±0.5	1.35	30.50	0.04

[a] Colloidal mass per kg of sample ±standard deviation (n=3)
[b] As and Fe concentrations in the CF per kg of colloid
[c] Molar ratio As/Fe of the DCF

Size distribution of the dispersible colloidal fraction and associated metal(loid)s

The DCF of the samples from the stream bed were measured by AF4-UV-Vis-ICP-MS. The colloidal size varies between 405nm (sample F) and 592nm (sample C). The DCF of A, B, E, and G show colloidal maxima close to 455nm (Table 9). The size characterization of the colloids associated with Al, Fe, and As shows similar values to each other for each sample analyzed. Likewise, higher recoveries are observed for the colloids associated with Al, Fe, and As in samples A, B, D, and E compared to the fractions measured by AF4-UV-Vis. The DCF leached from sample G shows a higher recovery than those of elements associated with colloids measured by AF4-ICP-MS, while samples F and C show similar recoveries by both ICP-MS and UV-Vis. The lowest colloidal recovery is obtained in sample C, while samples F and G show colloidal recoveries greater than 50% (Table 9).

Table 9. Mean values of colloidal size and recovery ratios in AF4 determinations of DCF

Sample	***AF4-UV-Vis***[a]		***AF4-ICP-MS***					
			Al		**Fe**		**As**	
	Size[b] *(nm)*	**Rec**[c] *(%)*	**Size**[b] *(nm)*	**Rec**[c] *(%)*	**Size**[b] *(nm)*	**Rec**[c] *(%)*	**Size**[b] *(nm)*	**Rec**[c] *(%)*
A	457	47.9	273	65.2	266	68.4	261	53.1
B	467	48.8	264	71.9	257	67.8	254	68.2
C	592	28.8	335	27.4	333	29.8	332	29.9
D	544	35.9	306	48.7	307	53.8	305	40.4
E	454	33.2	262	46.9	251	46.4	254	35.2
F	405	53.8	234	56.3	221	55.5	238	43.6
G	447	61.7	251	45.7	245	52.0	246	41.3

[a] Mean values of duplicated measures of DCF medios del análisis duplicado de la DCF
[b] Maximum value size distribution
[c] Recovery ratio (%) for each DCF

Geochemical modelling

Excluding adsorbed species, the MINEQL+ and Visual MINTEQ geochemical speciation programs predict scorodite ($FeAsO_4 \cdot 2H_2O$) and hematite (α-Fe_2O_3) as the thermodynamically favored phases, followed by schultenite ($PbHAsO_4$) and diaspore [α-AlO(OH)] in sample WP (Table 10). The model also suggests the presence of $AlSO_4^+$, $H_2AsO_4^-$, and $ZnSO_4$ in solution. Modeling using PHREEQC, and introducing the concentrations indicated in Table 10, yields similar results. Modeling the colloidal phase of WP revealed the greater stability of metals and metalloids in solution, except for Fe, whose precipitation as hematite or another colloidal Fe oxyhydroxide is clearly favored. Due to the high As concentration in the residue sample, all types of precipitated solid arsenates are predicted, being the scorodite the primary phase. The scorodite formation was not calculated in the WP colloidal sample due to the much lower As content. In this colloidal sample, the ratio between As and Fe concentrations is high enough (Table 8) to predict that the reactive groups on the surface of Fe(III) (hydr)oxides are saturated with respect to the total As(V) content. Therefore, it is likely that excess As(V) is adsorbed onto Fe oxides calculated by the model, causing the dissolved As(V) concentration to be lower than modeled. The percentage of dissolved As relative to colloidal As in WP is 13% (Table 7), while according to Visual MINTEQ and PHREEQC, all As should be dissolved (Table 10). Modeling of the colloidal residue indicates the prevalence of Fe oxyhydroxides as the only precipitated phase, which would adsorb the free AsO_4^{3-} present in the medium, causing most of the As (87%) to be transported associated with ≤1000nm colloidal Fe oxyhydroxides. In the stream bed, hematite and diaspore stand out as precipitated species, in addition to guerinite [$Ca_5H_2(AsO_4)_4 \cdot 9H_2O$] and $Zn_3(AsO_4)_2$. In samples B and D, the precipitation of baildonite [$PbCu_3(AsO_4)_2(OH)_2$] and $Cu_3(AsO_4)_2$ is also favored, while in sample F, the presence of hydroxymimetite [$Pb_5(AsO_4)_3OH$] is favored (Table 11). Comparing the results predicted by the system for the DCF of these samples, it is observed that the colloidal sample D has the highest levels of precipitated As (43.8%), with this value being lower in the colloidal samples B and F (close to 30%).

Table 10. Geochemical speciation in mine residue (WP) and its colloidal phase *(Visual MINTEQ)*

Mine residue (WP), pH=3.45, Ionic strenght=0.0056 M								
Al^{3+} [a]	**Fe^{3+}**	**Cu^{2+}**	**Zn^{2+}**	**As^{5+}**	**Pb^{2+}**	**Ca^{2+}**	**SO_4^{2-}**	**PO_4^{3-}**
(mol L-1)								
0.039	1.25	0.0058	0.006	0.29	0.016	0.001	0.0017	0.0002
Dissolved sp. [b]		**Precipitated sp.**			**Mass distribution**			
Specie	**Conc. *(M)***	**Specie**		**Conc.[c] *(M)***	**Specie**	**Dissolved *(%)***	**Precipitated *(%)***	
Al^{3+}	$7.2x10^{-4}$	$FeAsO_4 \cdot 2H_2O$		$2.7x10^{-1}$	Al^{3+}	4.6	95.4	
$AlHPO_4^+$	$1.3x10^{-4}$	α-Fe_2O_3 *d*		$4.8x10^{-1}$	Fe^{3+}	0	100	
$AlSO_4^+$	$8.8x10^{-4}$	$PbCu(AsO_4)OH$		$5.3x10^{-3}$	Cu^{2+}	9.0	91.0	
Cu^{2+}	$5.0x10^{-4}$	$PbHAsO_4$		$1.0x10^{-2}$	Zn^{2+}	100	0	
$H_2AsO_4^-$	$1.4x10^{-3}$	α-AlO(OH)		$3.7x10^{-2}$	AsO_4^{3-}	0.5	99.5	
SO_4^{2-}	$4.6x10^{-4}$	$Ca_5H_2(AsO_4)_4 \cdot 9H_2O$		$1.9x10^{-5}$	Pb^{2+}	0.1	99.9	
Zn^{2+}	$5.3x10^{-3}$				Ca^{2+}	6.7	93.3	
$ZnSO_4$	$2.8x10^{-4}$				SO_4^{2-}	100	0	
					PO_4^{3-}	100	0	

Table 10 (cont.). Geochemical speciation in mine residue (WP) and its colloidal phase *(Visual MINTEQ)*

Mine residue (WP) Colloidal, pH=3.45, Ionic strenght=0.0056 M								
Al^{3+a}	**Fe^{3+}**	**Cu^{2+}**	**Zn^{2+}**	**As^{5+}**	**Pb^{2+}**	**Ca^{2+}**	**SO_4^{2-}**	**PO_4^{3-}**
(mmol L-1)								
0.027	0.020	0.0035	0.006	0.0030	0.0002	1.85	31.8	0.00003
Dissolved sp. [b]		**Precipitated sp.**			**Mass distribution**			
Specie	**Conc. *(M)***	**Specie**		**Conc.[c] *(M)***	**Specie**	**Dissolved *(%)***	**Precipitated *(%)***	
$Al(SO_4)_2^-$	1.6x10-5	α-Fe_2O_3 [d]		1.0x10^{-5}	Al^{3+}	100	0	
$AlSO_4^+$	1.4x10-5				Fe^{3+}	0.02	99.98	
Ca^{2+}	3.9x10-4				Cu^{2+}	100	0	
$CaSO_4$	1.4x10-3				Zn^{2+}	100	0	
H_2CO_3	1.3x10-5				AsO_4^{3-}	100	0	
HSO_4^-	8.1x10-4				Pb^{2+}	100	0	
SO_4^{2-}	3.0x10-2				Ca^{2+}	100	0	
					SO_4^{2-}	100	0	
					PO_4^{3-}	100	0	

[a] Molar concentrations used for modelling
[b] Representative disolved species (>10^{-4}M soil samples and >10^{-5}M in colloid samples)
[c] Predicted solid concentration.
[d] Hematite

Table 11. Geochemical speciation of stream samples B, D, and F (Visual MINTEQ)

Sample B, pH=6.65, Ioinic Strenght=0.0013 M								
Al^{3+a}	**Fe^{3+}**	**Cu^{2+}**	**Zn^{2+}**	**As^{5+}**	**Pb^{2+}**	**Ca^{2+}**	**SO_4^{2-}**	**PO_4^{3-}**
(mol L^{-1})								
0.15	0.61	0.029	0.023	0.044	0.0022	0.0004	0.0002	0.0003
Dissolved sp.[b]		***Precipitated sp***			***Mass distribution***			
Specie	**Conc. *(M)***	**Specie**	**Conc.[c] *(M)***		**Specie**	**Dis-solved *(%)***	**Precipitated *(%)***	
$H_2AsO_4^-$	5.7x10^{-3}	α-AlO(OH)	1.5x10^{-1}		Al^{3+}	0	100	
$H_2PO_4^-$	2.2x10^{-4}	α-Fe_2O_3 [d]	3.1x10^{-1}		Fe^{3+}	0	100	
$HAsO_4^{2-}$	2.9x10^{-3}	$Ca_5H_2(AsO_4)_4 \cdot 9H_2O$	8.0x10^{-5}		Cu^{2+}	0	100	
SO_4^{2-}	2.0x10^{-4}	$Zn_3(AsO_4)_2$	7.8x10^{-3}		Zn^{2+}	0.2	99.8	
		$PbCu_3(AsO_4)_2OH_2$	2.2x10^{-3}		AsO_4^{3-}	19.4	80.6	
		$Cu_3(AsO_4)_2$	7.7x10^{-3}		Pb^{2+}	0	100	
					Ca^{2+}	0	100	
					SO_4^{2-}	100	0	
					PO_4^{3-}	100	0	

Table 11 (cont.). Geochemical speciation of stream samples B, D, and F (Visual MINTEQ)

Sample B colloidal, pH=6.65, Ionic Strenght=0.0013 M								
Al^{3+a}	Fe^{3+}	Cu^{2+}	Zn^{2+}	As^{5+}	Pb^{2+}	Ca^{2+}	SO_4^{2-}	PO_4^{3-}
(mmol L^{-1})[e]								
3.15	1.46	0.061	0.056	0.13	0.0077	0.0021	0.0008	0.0008

Dissolved sp.[b]		*Precipitated sp*		*Mass distribution*		
Specie	**Conc.** *(M)*	**Specie**	**Conc.[c]** *(M)*	**Specie**	**Dissolved** *(%)*	**Precipitated** *(%)*
$H_2AsO_4^-$	$6.0x10^{-5}$	α-AlO(OH)	$3.2x10^{-3}$	Al^{3+}	0	100
H_2CO_3	$1.3x10^{-5}$	α-Fe_2O_3	$7.3x10^{-4}$	Fe^{3+}	0	100
$HAsO_4^{2-}$	$3.1x10^{-5}$	$Ca_5H_2(AsO_4)_4 \cdot 9H_2O$	$4.0x10^{-7}$	Cu^{2+}	13.5	86.5
HCO_3^-	$2.7x10^{-5}$	$PbCu_3(AsO_4)_2OH_2$	$7.7x10^{-6}$	Zn^{2+}	100	0
Zn^{2+}	$6.0x10^{-5}$	$Cu_3(AsO_4)_2$	$9.9x10^{-6}$	AsO_4^{3-}	71.3	28.7
				Pb^{2+}	0	100
				Ca^{2+}	0	100
				SO_4^{2-}	100	0
				PO_4^{3-}	100	0

Sample D, pH=6.69, Ionic Strenght=0.0007 M								
Al^{3+a}	Fe^{3+}	Cu^{2+}	Zn^{2+}	As^{5+}	Pb^{2+}	Ca^{2+}	SO_4^{2-}	PO_4^{3-}
(mol L^{-1})								
0.11	0.41	0.022	0.018	0.031	0.0017	0.0002	0.0002	0.0002

Dissolved sp.[b]		*Precipitated sp*		*Mass distribution*		
Specie	**Conc.** *(M)*	**Specie**	**Conc.[c]** *(M)*	**Specie**	**Dissolved** *(%)*	**Precipitated** *(%)*
$H_2AsO_4^-$	$2.5x10^{-3}$	α-AlO(OH)	$1.9x10^{-1}$	Al^{3+}	0	100
$H_2PO_4^-$	$1.5x10^{-4}$	α-Fe_2O_3	$2.0x10^{-1}$	Fe^{3+}	0	100
$HAsO_4^{2-}$	$1.4x10^{-3}$	$Ca_5H_2(AsO_4)_4 \cdot 9H_2O$	$4.0x10^{-5}$	Cu^{2+}	0.1	99.9
SO_4^{2-}	$2.0x10^{-4}$	$Zn_3(AsO_4)_2$	$6.0x10^{-3}$	Zn^{2+}	0.4	99.6
		$PbCu_3(AsO_4)_2OH_2$	$1.7x10^{-3}$	AsO_4^{3-}	12.6	87.4
		$Cu_3(AsO_4)_2$	$5.6x10^{-3}$	Pb^{2+}	0	100
				Ca^{2+}	0	100
				SO_4^{2-}	100	0
				PO_4^{3-}	100	0

Sample D coloidal, pH=6.69, Ionic Strenght=0.0007 M								
Al^{3+a}	Fe^{3+}	Cu^{2+}	Zn^{2+}	As^{5+}	Pb^{2+}	Ca^{2+}	SO_4^{2-}	PO_4^{3-}
(mmol L^{-1}) [e]								
2.53	0.98	0.075	0.063	0.10	0.0070	0.0011	0.001	0.0006

Dissolved sp.[b]		*Precipitated sp*		*Mass distribution*		
Specie	**Conc.** *(M)*	**Specie**	**Conc.[c]** *(M)*	**Specie**	**Dissolved** *(%)*	**Precipitated** *(%)*
$H_2AsO_4^-$	$3.7x10^{-5}$	αAlO(OH)	$2.5x10^{-3}$	Al^{3+}	0	100
H_2CO_3	$1.3x10^{-5}$	α-Fe_2O_3	$4.9x10^{-4}$	Fe^{3+}	0	100
$HAsO_4^{2-}$	$2.0x10^{-5}$	$Ca_5H_2(AsO_4)_4 9H_2O$	$2.0x10^{-7}$	Cu^{2+}	13.2	86.8
HCO_3^-	$2.9x10^{-5}$	$PbCu_3(AsO_4)_2OH_2$	$7.0x10^{-6}$	Zn^{2+}	100	0
Zn^{2+}	$6.0x10^{-5}$	$Cu_3(AsO_4)_2$	$1.5x10^{-5}$	AsO_4^{3-}	56.2	43.8
				Pb^{2+}	0	100
				Ca^{2+}	0	100
				SO_4^{2-}	100	0
				PO_4^{3-}	100	0

Table 11 (cont.). Geochemical speciation of stream samples B, D, and F (Visual MINTEQ)

Sample F, pH=6.54, Ionic Strenght=0.0009 M								
Al^{3+a}	Fe^{3+}	Cu^{2+}	Zn^{2+}	As^{5+}	Pb^{2+}	Ca^{2+}	SO_4^{2-}	PO_4^{3-}
(mol L^{-1})								
0.091	0.38	0.006e	0.020	0.011	0.0008	0.0004	0.0001	0.0002

Dissolved sp.[b]		*Precipitated sp*		*Mass distribution*		
Specie	**Conc.** *(M)*	**Specie**	**Conc.[c]** *(M)*	**Specie**	**Dissolved** *(%)*	**Precipitated** *(%)*
Zn^{2+}	$5.0x10^{-3}$	αAlO(OH)	$9.1x10^{-2}$	Al^{3+}	0	100
$ZnHPO_4$	$1.2x10^{-4}$	αFe_2O_3	$1.9x10^{-1}$	Fe^{3+}	0	100
		$Ca_5H_2(AsO_4)_4 \cdot 9H_2O$	$8.0x10^{-5}$	Cu^{2+}	-	-
		$Pb_5(AsO_4)_3OH$	$1.6x10^{-4}$	Zn^{2+}	25.4	74.6
		$Zn_3(AsO_4)_2$	$5.1x10^{-3}$	AsO_4^{3-}	0.1	99.9
				Pb^{2+}	0.01	99.99
				Ca^{2+}	0	100
				SO_4^{2-}	100	0
				PO_4^{3-}	100	0

Sample F colloidal, pH=6.54, Ionic Strenght=0.0009M								
Al^{3+a}	Fe^{3+}	Cu^{2+}	Zn^{2+}	As^{5+}	Pb^{2+}	Ca^{2+}	SO_4^{2-}	PO_4^{3-}
(mol L^{-1})								
2.82	0.84	0.014	0.067	0.031	0.0029	0.0042	0.001	0.0001

Dissolved sp. [b]		*Precipitated sp*		*Mass distribution*		
Specie	**Conc.** *(M)*	**Specie**	**Conc.[c]** *(M)*	**Specie**	**Dissolved** *(%)*	**Precipitated** *(%)*
$H_2AsO_4^-$	$1.6x10^{-5}$	αAlO(OH)	$2.8x10^{-3}$	Al^{3+}	0	100
H_2CO_3	$1.3x10^{-5}$	αFe_2O_3	$4.2x10^{-4}$	Fe^{3+}	0	100
HCO_3^-	$2.1x10^{-5}$	$Ca_5H_2(AsO_4)_4 \cdot 9H_2O$	$8.0x10^{-7}$	Cu^{2+}	37.86	62.14
Zn^{2+}	$7.0x10^{-5}$	$PbCu_3(AsO_4)_2OH_2$	$2.9x10^{-6}$	Zn^{2+}	100	0
				AsO_4^{3-}	70.97	29.03
				Pb^{2+}	0	100
				Ca^{2+}	0	100
				SO_4^{2-}	100	0
				PO_4^{3-}	100	0

[a] Molar concentrations used for modelling
[b] Representative disolved species (>10^{-4}M soil samples and >10^{-5}M in colloid samples)
[c] Predicted solid concentration.
[d] Hematite

Discussion

Arsenic dispersion in soils adjacent to the stream bed

The concentrations measured in soil samples reveal significant contamination of the area not only by As, but also by other toxic elements such as Cu and Pb, resulting from the accumulation of mine residues rich in arsenopyrite. EXAFS spectroscopy indicates differences in As and Fe speciation in the samples studied (Table 3). The mining residue shows a significant contribution of mixed Fe(II)/Fe(III) oxides, indicative of the oxidation of pyritic residues, which causes the co-precipitation of the two Fe species in a single mineral phase. In sample B, representative of the runoff area near the residue, the importance of the hydrous ferric oxide nanomineral, ferrihydrite as an adsorbent phase for As released

by arsenopyrite oxidation is observed. In contrast, samples D and F show a more significant contribution of goethite as a phase associated with free As than ferrihydrite. The greater thermodynamic stability of goethite [α-FeO(OH)] compared to ferrihydrite causes the transition from one phase to another, although ferrihydrite formation may be initially favored, as also indicated in the geochemical modeling performed. The presence of schwertmannite in the stream bed soil samples (Fe EXAFS) confirms the transition that pyritic residues undergo towards oxidized hydroxysulfates such as schwertmannite and jarosite (Murad and Rojik, 2005).

These results highlight the importance of ferrihydrite as an initial As carrier once arsenopyrite residues dissolve, due to its high As(V) adsorption capacity (Fritzsche et al., 2011). A significant decrease in As concentration is observed as the distance from the contamination source increases, especially in the two furthest samples, F and G (Table 3). This reduction in As may be due to the dissolution of As carriers, releasing As through preferential flows in the stream bed (Helmhart et al., 2012) (Table 4), causing As to remain associated only with the most stable phases, such as crystalline Fe(III) oxyhydroxides or hydroxysulfates. The decrease in the As/Fe molar ratio in soil samples along the stream bed (Table 3) confirms the importance of Fe phases as the distance from the contamination source increases.

As mobilization in colloidal phases

The mobilization of colloidal As from the residue occurs through a mixture of three mineral components: ferrihydrite, scorodite, and goethite. The presence of scorodite is explained by the tendency of these secondary arsenates to form due to natural oxidation in soils with high arsenopyrite concentrations. Furthermore, the formation of colloidal goethite and Fe hydroxysulfates is thermodynamically favored by their higher crystallinity compared to less crystalline phases, while the ferrihydrite is more favored kinetically.

On the other hand, the As EXAFS analysis for the CF of the stream bed samples indicates a significant mobilization of As associated with ferrihydrite colloids. This trend is supported by the EXAFS of the colloidal sample B, as it is a transition zone near the residue, where ferrihydrite has not yet transformed into a more stable Fe oxyhydroxide. The significant formation of hydroxysulfates such as schwertmannite and jarosite (or plumbojarosite) detected in the colloidal samples confirms the results obtained by EXAFS as well as the tendency of pyritic residues to form this type of colloidal mineral phases (Murad and Rojik, 2005).

The As concentration in colloidal samples from the stream bed indicates that the vast majority of As in the DCF is found in the solids of the CF (Table 7). The geochemical modeling predicts that 29-44% of As should be precipitated under these conditions, inferred to occur as As minerals of small particle sizes. Therefore, more than 56% of the leaching As could be mobilized as adsorbed species onto colloidal Fe oxides and/or aluminosilicates. For the other elements studied, the system suggests that Al, Fe, and Pb should be precipitated entirely, which is consistent with the quantifications performed. Likewise, between 12-30% of Cu should be in the dissolved fraction according to the model, although the quantifications performed indicate that most of the Cu is in the colloidal phase and not in the dissolved fraction. Therefore, we infer that the above percentage must be sorbed to small mineral particles. Geochemical modeling is beneficial for predicting thermodynamically favored mineral phases based on their precipitation constants, but it does not include sorption processes unless specifically designated reactions are entered in their databases. Furthermore, the guerinite [$Ca_5H_2(AsO_4)_4 \cdot 9H_2O$] species described in the geochemical model cannot be detected by other instrumental techniques such as XRD or XAS (Martinez-Villegas et al., 2013), making it impossible to confirm its presence in the samples. To carry out a comprehensive and in-depth study of the system, adsorption processes and possible redox processes resulting from the weathering and erosion of soils due to rain and surface runoff must also be considered (Gomez-Gonzalez et al., 2016). Therefore, the modeling described here can be used to predict the stable phases according to the chemical equilibrium reached depending on the soil pH and ionic strength. However, the distribution of adsorbed elements onto other species can vary.

As speciation in soils vs colloids

One of the unique aspects of this work is the direct study of the As-bearing phases and other trace elements in the bulk soils adjacent to the contaminated area and their corresponding readily mobilizable colloidal fractions. XAS spectroscopy indicates that the As speciation in the soils is practically identical to that in the colloidal fraction for samples WP, B, and F, which show ferrihydrite as the primary As-carrying phase (in addition to scorodite in the case of the residue). Colloidal samples D and G show a small contribution of adsorption to goethite in addition to this mobilization mechanism. These results are within expectations (and consistent with geochemical modeling), supporting the initial adsorption of As by nanoparticulate ferrihydrite, which subsequently crystallizes into a more stable form such as goethite. Fe EXAFS, on the other hand, indicates the presence of scorodite, a mixed Fe(II)/Fe(III) oxide in the spoil heap (WP), and a mixture of illite and hydroxysulfates (schwertmannite) in the soil samples collected along the stream bed. The Fe colloidal phases continue to show this mixture of smectite, illite, and hydroxysulfates (schwertmannite), along with significant contributions of ferrihydrite (in sample B) and plumbojarosite (in WP, D, and F). The most significant variation between a solid sample and the colloidal phase is observed in the spoil heap (WP). Notably, scorodite is not detected in the Fe EXAFS analyses carried out on the WP colloidal fraction, although it is the primary phase in the Fe EXAFS of the solid residue. However, the major presence of smectite in the area (especially in its clay fraction) may mask the presence of colloidal scorodite in the case of Fe EXAFS analyses because smectite may contain large fractions of Fe, unlike As EXAFS analyses, which do indicate the mobilization of colloidal scorodite.

Starting from the DCF concentrations, the colloidal concentrations in mg As kg^{-1} colloid can be compared with the soil sample concentrations. In the case of the spoil heap (WP and WP-2), only 0.01% of the As is mobilized with the colloidal matter, while in samples A-B-D-E-F, between 2.6–3.2% of the As is associated with the colloid. Similar percentages of Fe, Cu, Zn, and Pb are mobilized by the colloidal matter in these areas. On the other hand, between 20-33% of aluminum (Al) is mobilized in the stream's colloids, indicating the importance of aluminosilicates in the ≤1000nm colloidal fraction. When comparing these results with those described in Serrano et al. (2015), a similar percentage of As associated with the colloidal fraction from the mining residue (0.04%) is obtained. However, in that work, a greater mobilization of colloidal As, up to 35% in stream bed soils, is observed, although in their case, the samples are closer in distance to the mining residue than in the present work, where the permanent stream flow causes As to be mobilized more continuously, making it less available for the leaching tests carried out in our studies.

The complementary analyses carried out on the natural runoff waters of the area show significant levels of As, Mn, Tl, and Pb along the quasi-permanent stream flow, highlighting the evident environmental risk associated with the presence of mining residues exposed to precipitation and surface runoff.

Conclusions

The characterization of solid sediments and associated dispersible colloidal fractions using multiple and complementary analytical techniques allows us to draw the following conclusions: i) there is a high colloidal As mobilization from the mining residue that affects the soils adjacent to the nearby natural stream up to a distance of almost 1 km from the contamination source. However, the importance of this colloidal As relative to the total As in the sediment is only 2.6-3.2%, which, although seemingly low, could justify the contamination levels found in areas far from the residues due to continuous release; ii) colloidal Fe oxyhydroxides play an important role in As mobilization. In areas near the mining residue, less crystalline and nanometer-sized oxyhydroxides tend to form, while as they advance along the flowing stream, these As carriers are more crystalline; and iii) the nature of the dispersible colloidal phases depends on the sediment from which they originate, but once released, they undergo mineral transformations. This behavior influences the overall As transport process, as the more stable crystalline vectors show more potential for contaminant diffusion and can move to areas further from the residue.

DECLARATION OF CONFLICT OF INTERESTS

The authors of this article declare that they have no financial, professional, or personal conflicts of interest that could have inappropriately influenced this work.

FINANCIAL SUPPORT

This work was funded by the Spanish Government (CGL2010-17434) and the Government of Aragon (E29_23R). XAS measurements on BM25A beamline (ESRF) supported by the 25-01-944 project. The authors acknowledge the use of the General Research Support Service-SAI, University of Zaragoza. M.V. is grateful to DGAPA PAPIIT Project IN104923 in Mexico for the funds provided.

CRediT AUTHORSHIP

Miguel Angel Gomez-Gonzalez: Investigación, Metodología, Análisis de Datos, Visualización, Redacción – borrador original; **Fernando Garrido**: Conceptualización, Adquisición De Financiación, Administración de Proyectos, Revisión, Redacción – Revisión y Edición; **Francisco Laborda**: Conceptualización, Metodología, Investigación, Redacción – Revisión y Edición; **Mario Villalobos**: Conceptualización, Metodología, Investigación, Redacción – Revisión y Edición; **Eduardo Bolea**: Conceptualización, Metodología, Investigación, Redacción – Revisión y Edición; **Paula Gómez-Arce**: Análisis Formal, Redacción – Revisión y Edición; **Javier Aguilar-Carrillo**: Análisis Formal, Redacción – Revisión y Edición.

References

Bolea, E., Laborda, F. & Castillo, J. R. (2010). Metal associations to microparticles, nanocolloids and macromolecules in compost leachates: Size characterization by asymmetrical flow field-flow fractionation coupled to ICP-MS. *Analytica Chimica Acta*, 661, 206-214. https://doi.org/10.1016/j.aca.2009.12.021

Cánovas, C. R., Macías, F., Basallote, M. D., Olías, M., Nieto., J. M. & Pérez-López, R. (2021). Metal(loid) release from sulfide-rich wastes to the environment: The case of the Iberian Pyrite Belt (SW Spain). *Curret Opinion in Environmental Sciene & Health*, 20, 100240. https://doi.org/10.1016/j.coesh.2021.100240

Chen M. & Ma, L. Q. (2001). Comparison of three aqua regia digestion methods for twenty Florida soils. *Soil Science Society of America Journal*, 65, 491-499. https://doi.org/10.2136/sssaj2001.652491x

Courtin-Nomade, A., Waltzing, T., Evrard, C., Soubrand, M., Lenain, J.F., Ducloux, E., Ghorbel, S., Grosbois, C. & Bril, H. (2016). Arsenic and lead mobility: from tailing materials to the aqueous compartment. *Applied Geochemistry*, 64, 10-21. https://doi.org/10.1016/j.apgeochem.2015.11.002

Fritzsche, A., Rennert, T. & Totsche, K.U. (2011). Arsenic strongly associates with ferrihydrite colloids formed in a soil effluent. *Environmental Pollution*, 159, 1398-1405. https://doi.org/10.1016/j.envpol.2011.01.001

Gomez-Gonzalez, M. A., Garcia-Guinea, J., Laborda, F. & Garrido, F. (2015). Thallium occurrence and partitioning in soils and sediments affected by mining activities in Madrid province (Spain). *Science of the Total Environment*, 536, 268-278. https://doi.org/10.1016/j.scitotenv.2015.07.033

Gomez-Gonzalez, M. A., Voegelin, A., Garcia-Guinea, J., Bolea, E., Laborda, F. & Garrido, F. (2016). Colloidal mobilization of arsenic from mining-affected soils by surface runoff. *Chemosphere*, 144, 1123-1131. https://doi.org/10.1016/j.chemosphere.2015.09.090

Gomez-Gonzalez, M. A., Villalobos, M. Marco, J. F., Garcia-Guinea, J., Bolea, E., Laborda, F., Garrido, F. (2018). Iron oxide - clay composite vectors on long-distance transport of arsenic and toxic metals in mining-affected areas. *Chemosphere*, 197, 759-767. https://doi.org/10.1016/j.chemosphere.2018.01.100

Gustafsson, J. P. (2010). *Visual MINTEQ - A free equilibrium speciation model software*. KTH, Department of Sustainable Development, Environmental Science and Engineering.

Helmhart, H., O'Day, P. A., Garcia-Guinea, J., Serrano, S. & Garrido F. (2012) Arsenic, Copper, and Zinc Leaching through Preferential Flow in Mining-Impacted Soils. *Soil Science Society of America Journal*, 76, 449-462. https://doi.org/10.2136/sssaj2011.0269

Hu, P., Zhang, Y., Wang, J., Du, Y., Wang, A., Guo, Q., Pan, Z., Ma, X., Planer-Friedich, B., Luo, Y. & Wu, L. (2023). Mobilization of colloid- and nanoparticle-bound arsenic in contaminated paddy soils during reduction and reoxidation. *Environmental Science & Technology*, 57, 9843-9853. https://doi.org/10.1021/acs.est.3c03051

Jimenez, R., Jorda, L., Jorda, R. & Prado, P. (2004). La minería metálica en Madrid. *Botanica*, 14, 50-89.

Kretzschmar, R., Borkovec, M., Grolimund, D. & Elimelech, M. (1999). Mobile subsurface colloids and their role in contaminant transport. *Advances in Agronomy*, 66 121-193. https://doi.org/10.1016/S0065-2113(08)60427-7

Laborda, F., Ruiz-Beguería, S., Bolea, E. & Castillo, J. R. (2011). Study of the size-based environmental availability of metals associated to natural organic matter by stable isotope exchange and quadrupole inductively coupled plasma mass spectrometry coupled to asymmetrical flow field flow fractionation. *Journal of Chromatography A*, 1218, 4199-4205. https://doi.org/10.1016/j.chroma.2011.01.076

Martin-Crespo, T., Vindel, E., Lopez-Garcia, J. A. & Cardellach, E. (2004). As-(Ag) sulphide veins in the Spanish Central System: further evidence for a hydrothermal event of Permian age. *Ore Geology Reviews*, 25, 199-219. https://doi.org/10.1016/j.oregeorev.2004.04.007

Martinez-Villegas, N., Briones-Gallardo, R., Ramos-Leal, J. A., Avalos-Borja, M., Castanon-Sandoval, A. D., Razo-Flores, E. & Villalobos, M. (2013). Arsenic mobility controlled by solid calcium arsenates: A case study in Mexico showcasing a potentially widespread environmental problem. *Environmental Pollution*, 176,114-122. https://doi.org/10.1016/j.envpol.2012.12.025

Moreno-Jimenez, E., Peñalosa, J. M., Manzano, R., Carpena-Ruiz, R. O., Gamarra, R. Esteban, E. (2009). Heavy metals distribution in soils surrounding an abandoned mine in NW Madrid (Spain) and their transference to wild flora. *Journal of Hazardous Material*, 162, 854-859. https://doi.org/10.1016/j.jhazmat.2008.05.109

Murad, E. & Rojik, P. (2005). Iron mineralogy of mine-drainage precipitates as environmental indicators: review of current concepts and a case study from the Sokolov Basin, Czech Republic. *Clay Minerals*, 40, 427-440. https://doi.org/10.1180/0009855054040181

O'Day, P. A., Vlassopoulos, D., Root, R. & Rivera, N. (2004). The influence of sulfur and iron on dissolved arsenic concentrations in the shallow subsurface under changing redox conditions. *Proceedings of the National Academy of Sciences (U.S.A)*, 101, 13703-13708. https://doi.org/10.1073/pnas.0402775101

Parkhurst, D. L. & Appelo, C. A. (1999). *User's Guide to PHREEQC (Version 2)-A Computer Program for Speciation, Batch-Reaction, One-Dimensional Transport, and Inverse Geochemical Calculations*. United States Geological Survey, Water Resources Investigations Report 99-4259.

Plathe, K. L., von der Kammer, F., Hassellov, M., Moore, J., Murayama, M., Hofmann, T. & Hochella, M. F. (2010). Using FlFFF and aTEM to determine trace metal-nanoparticle associations in riverbed sediment. *Environmental Chemistry*, 7, 82-93. https://doi.org/10.1071/EN09111

Ravel, B. & Newville, M. (2005). ATHENA, ARTEMIS, HEPHAESTUS: data analysis for Xray absorption spectroscopy using IFEFFIT. *Journal of Synchrotron Radiation*, 12, 537-541. https://doi.org/10.1107/S0909049505012719

Schecher, W. D. & McAvoy, D.C. (1992). MINEQL+ - A software environment for chemical-equilibrium modeling, *Computers Environment and Urban Systems*, 16, 65-76. https://doi.org/10.1016/0198-9715(92)90053-T

Serrano, S., Gomez-Gonzalez, M. A., O'Day, P. A., Laborda, F., Bolea, E. & Garrido, F. (2015). Arsenic speciation in the dispersible colloidal fraction of soils from a mine-impacted creek. *Journal of Hazard Materials*, 286, 30-40. https://doi.org/10.1016/j.jhazmat.2014.12.025

Villalobos, M., García-Payne, D. G., Lopez-Zepeda, J. L., Ceniceros-Gomez, A. E. & Gutierrez-Ruiz, M. E. (2010). Natural arsenic attenuation via metal arsenate precipitation in soils contaminated with metallurgical wastes: I. Wet chemical and thermodynamic evidences. *Aquatic Geochemistry*, 16, 225-250. https://doi.org/10.1007/s10498-009-9065-4

Walkley, A. & Black, I. A. (1934). An examination of the Degtjareff method for determining soil organic matter, and a proposed modification of the chromic acid titration method. *Soil Science*, 37, 29-38. https://doi.org/10.1097/00010694-193401000-00003